

A HYBRID FINITE-VOLUME/FINITE-DIFFERENCE SCHEME FOR ONE-DIMENSIONAL BOUSSINESQ EQUATIONS TO SIMULATE WAVE ATTENUATION DUE TO VEGETATION

Soumendra Nath Kuiry¹, Weiming Wu², and Yan Ding³

Abstract: A numerical scheme to solve the extended one-dimensional Boussinesq equations with the effects of vegetation is presented. The finite-volume method based on the HLL Riemann solver is used to discretize the conservative part of the equations, while the finite-difference method is used to discretize the remaining terms. The values of the variables at an interface for the use in the local Riemann problem are computed by a fourth-order MUSCL reconstruction technique. The bed slope, bed friction, resistance due to vegetation and Boussinesq terms are discretized using centered finite-difference schemes of up to fourth-order accuracy. The unsteady term is discretized by the second-order MUSCL-Hancock scheme unlike the previous schemes such as Adams-Brashforth or Adams-Moulton where a fourth-order method is used thus saving storage and computational resources. The depth variable is evaluated explicitly by solving the continuity equation. The effects of vegetation are added in the source terms of the momentum equation in the form of drag. The drag force is due to the resistance offered by the vegetation to the flowing water. The momentum equation is then arranged in such a way that the Riemann solver can be applied for the conservative part. The resulting discretized equation form a tri-diagonal matrix which is solved efficiently by the Thomas algorithm. The use of Riemann solver makes the model capable of capturing shocks and is therefore suitable for simulating both breaking and non-breaking waves from deep to shallow water regions. Nevertheless, the presented Boussinesq model can easily be reduced to depth-averaged shallow water model by simply setting still water depth equals to zero. The proposed model is validated against various experimental observations. The comparison results prove that the hybrid model is suitable for predicting wave propagation and attenuation due to vegetation.

Keywords: Boussinesq equations, HLL Riemann solver, Effects of vegetation, Wave propagation, Wave attenuation, Fourth-order accuracy.

¹ Ph. D., Research Scientist, National Center for Computational Hydroscience and Engineering, The University of Mississippi, University, MS 38677, Email: snkuiry@ncche.olemiss.edu

² Ph.D., Research Associate Professor, National Center for Computational Hydroscience and Engineering, The University of Mississippi, University, MS 38677, Email: wuwm@ncche.olemiss.edu

³ Ph. D., A. M. ASCE, Research Assistant Professor, National Center for Computational Hydroscience and Engineering, The University of Mississippi, University, MS 38677, Email: ding@ncche.olemiss.edu

INTRODUCTION

The global climate change and manmade factors have resulted in developing extreme hydrological conditions such as storm surge, typhoon, tornado etc. The long waves generated by extreme hydrological conditions may develop large amplitudes in coastal water and inundate low-lying areas causing coastal barrier breaching, casualties and damage to properties. The growth of vegetations in these areas is favored. Vegetation protects the shoreline through the root systems and enhances the storage of sand in dunes. Nevertheless, waves propagating over vegetation will be attenuated due to resistance offered by vegetation. Therefore, vegetation plays a significant role on wave run-up and attenuation and shoreline stability.

The quantification of wave run-up and attenuation due to vegetation can be achieved by using numerical models which can be validated by conducting laboratory and field measurements. Numerical modeling of free surface flows described by the Navier-Stokes equations has received much interest in the latter half of the twentieth century. Due to complexity and computational resources required to solve the full Navier-Stokes equations, a depth-averaged assumption is used to simplify the governing equations so that the numerical model can be of practical use. In further simplification, the one-dimensional form of the depth-averaged equations is used for many engineering purposes. Unfortunately, the shallow water equations are not applicable for modeling wave propagation in relatively deep water and when the propagating waves are short in nature. In these circumstances, the extended Boussinesq equations can be a suitable choice.

The pioneer work of Peregrene (1967) provides the foundation for many Boussinesq type models used today. Madsen et al. (1991), Madsen and Sørensen (1992) and Nwogu (1993) enhanced the classical Boussinesq equations. The former introduces third-order terms with a free parameter into the momentum equation, while the latter derives a new set of governing equations from the three-dimensional Euler equations with the horizontal velocity evaluated at a reference depth. The two approaches have identical dispersion characteristics that show good agreement with linear wave theory. When effects of vegetation are lumped into the source term of the momentum equation, the system of equations can be used to simulate wave run-up and attenuation due to vegetation. The modified form of the Boussinesq equations presented by Madsen and Sørensen (1992) is considered in the present study.

A shock-capturing form of the one-dimensional Boussinesq equations is modeled to predict wave run-up and attenuation due to vegetation. The flux term is discretized by finite volume based fourth-order accurate scheme. The dispersion and source terms are discretized by centered finite-difference method. The unsteady term is discretized by second-order MUSCL-Hancock scheme. The drag force offered by vegetation is considered as source term in the momentum equation. The hybrid finite-volume/finite-difference scheme is validated against laboratory experiments and the comparisons prove the effectiveness of the proposed model.

GOVERNING EQUATIONS

In this section the extended Boussinesq equations of Madsen and Sørensen (1992) are presented and rewritten in the conservative form so that a hybrid finite-volume/finite-difference scheme can be used. Figure 1 provides the definition sketch of the free surface flow problem, in which h denotes the water depth, η the free surface elevation, and $h = d + \eta$ the flow depth. The equations derived by Madsen and Sørensen (1992) are:

$$\frac{\partial \eta}{\partial t} + \frac{\partial(hu)}{\partial x} = 0 \quad (1)$$

$$\frac{\partial(hu)}{\partial t} + \frac{\partial(hu^2)}{\partial x} + gh \frac{\partial \eta}{\partial x} + \frac{\partial \psi}{\partial x} = 0 \quad (2)$$

where u is the depth-averaged horizontal velocity and ψ are the terms that model dispersion:

$$\frac{\partial \psi}{\partial x} = - \left(B + \frac{1}{3} \right) d^2 \frac{\partial^3(hu)}{\partial x^2 \partial t} - Bgd^3 \frac{\partial^3 \eta}{\partial x^3} - d \frac{\partial d}{\partial x} \left(\frac{1}{3} \frac{\partial^2(hu)}{\partial x \partial t} + 2Bgd \frac{\partial^2 \eta}{\partial x^2} \right) \quad (3)$$

In Eq. (3), B is a free parameter that determines the dispersion properties of the system. Madsen and Sørensen has suggested a value of $B = 1/15$. Since the bathymetry remains constant over time, the Eqs. (1) and (2) can be written in the conservative form:

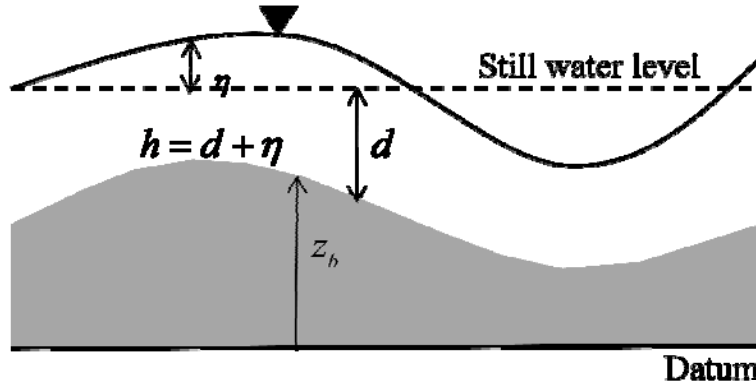


Figure 1. Definition sketch of free surface flow

$$\frac{\partial \mathbf{U}}{\partial t} + \frac{\partial \mathbf{F}(\mathbf{U})}{\partial x} = \mathbf{S} \quad (4)$$

where \mathbf{U} and $\mathbf{F}(\mathbf{U})$ are vectors containing the conserved variables and fluxes respectively, \mathbf{S} is the vector of source terms and are given by

$$\mathbf{U} = \begin{bmatrix} h \\ U(hu) \end{bmatrix}; \quad \mathbf{E} = \begin{bmatrix} hu \\ hu^2 + \frac{1}{2}gh^2 \end{bmatrix}; \quad \mathbf{S} = \begin{bmatrix} 0 \\ gh(S_o - S_f) - F_D + S_d \end{bmatrix} \quad (5)$$

where

$$U(hu) = hu - \left(B + \frac{1}{3}\right) d^2 \frac{\partial^2(hu)}{\partial x^2} - \frac{1}{3} d \frac{\partial d}{\partial x} \frac{\partial(hu)}{\partial x} \quad (6)$$

The source terms are given by

$$S_o = gh \frac{\partial d}{\partial x}; \quad S_f = \frac{n^2 u |u|}{h^{4/3}}; \quad F_D = \frac{1}{2} C_D N_v A_v d u |u| \quad (7)$$

$$S_d = Bgd^3 \frac{\partial^3 \eta}{\partial x^3} + 2Bgd^2 \frac{\partial d}{\partial x} \frac{\partial^2 \eta}{\partial x^2}$$

where S_o is the bed slope, S_f is the friction slope, F_D defines the drag force per unit area induced by vegetation, and S_d is the dispersion term. The coefficient of friction is denoted by n , C_D is the drag coefficient, N_v denotes number of stems per unit area and A_v is the projected area of a stem normal to flow direction given by

$$A_v = b_v \min(h_v, h) \quad (8)$$

in which b_v is width of stem, h_v is length of stem and t_v is thickness of stem.

NUMERICAL FORMULATION

The numerical scheme used to solve the governing equations is a fourth-order accurate in space, second-order accurate in time hybrid finite-volume/finite-difference scheme. The governing Eq. (4) is integrated over a cell length, Δx and the divergence theorem is applied to obtain conservation laws of mass and momentum:

$$\int_{\Delta x} \frac{\partial \mathbf{U}}{\partial t} dx + \oint_{\Gamma} \mathbf{F} \cdot \mathbf{n}_m d\Gamma = \int_{\Delta x} \mathbf{S} dx \quad (9)$$

where \mathbf{n}_m is the outward pointing normal vector to side m . The flux and source term computations are explained in the following sections.

Riemann fluxes

The finite volume formulation requires the solution of a local Riemann problem at each cell interface and therefore, the HLL Riemann solver (Harten et al. 1983) is used here to compute the convective fluxes. The HLL Riemann solver is preferred

because it better describes the flux for dry bed situation and does not require any entropy fix (Toro 1992). Wei and Kirby (1995) pointed out that a fourth-order accurate treatment of the first-order derivatives was required so that the truncation error in the numerical scheme is smaller than the dispersion terms present in the model. In order to calculate the conserved variables at each cell interface for the Riemann flux computation, the fourth-order MUSCL reconstruction proposed by Yamamoto et al. (1998) is implemented in this study. For smooth reconstruction method of water surface at a cell interface, the surface gradient method (Zhou et al. 2001) is followed.

Source terms

A cell-centered discretization is used for the bed slope, friction and vegetation terms. The first-order derivative is evaluated using fourth-order central difference approximation and second- and third-order central differences for the second- and third-order spatial derivatives present in the dispersion terms. The discretized source term takes the following form

$$S_i = -gh_i \left(\frac{z_{bi+1/2} - z_{bi-1/2}}{\Delta x} \right) - gh_i S_f - F_D + \frac{Bgd_i^3}{2\Delta x^3} (-\eta_{i-2} + 2\eta_{i-1} - 2\eta_{i+1} + \eta_{i+2}) + \frac{Bgd_i^3}{6\Delta x^3} (d_{i-2} - 8d_{i-1} + 8d_{i+1} - d_{i+2})(\eta_{i-1} - 2\eta_i + \eta_{i+1}) \quad (11)$$

Time integration

The time discretization is generally based on high-order predictor and corrector approach. A popular discretization proposed by Wei and Kirby (1995) is the third-order Adams-Brashforth for predictor and fourth-order Adams-Moulton for corrector. Shiach and Mingham (2009) proved that second-order accurate MUSCL-Hancock scheme provides sufficient accuracy and hence it is adopted in this study. This scheme uses two-stage predictor-corrector method. The predictor step determines the intermediate values over a half time step as

$$\mathbf{U}^{t+1/2} = \mathbf{U}^t - \frac{\Delta t}{2\Delta x} \left[\sum_{m=1}^M \mathbf{F}(\mathbf{U}_m)^t \cdot \mathbf{n}_m \right] \quad (12)$$

where t and $t + 1/2$ denote the current and intermediate values, M is the number of sides of the finite volume cell and Δt is the time step. The corrector steps provides the full conservative solution over a time step and is given by

$$\mathbf{U}^{t+1} = \mathbf{U}^t - \frac{\Delta t}{\Delta x} \left[\sum_{m=1}^M \mathbf{F}(\mathbf{U}_m^L, \mathbf{U}_m^R)^{t+1/2} \cdot \mathbf{n}_m \right] + \Delta t \left[gh(S_o - S_f) - F_D + S_d \right] \quad (13)$$

where $\mathbf{F}(\mathbf{U}_m^L, \mathbf{U}_m^R)$ is the flux at the cell interface m , the values of which are obtained by the HLL Riemann solver and \mathbf{U}_m^L and \mathbf{U}_m^R the values of the conserved

variables at the cell interface obtained by the fourth-order MUSCL reconstruction method proposed by Yamamoto et al. (1998).

Evaluation of Velocity

In order to discretize Eq. (6), a second-order accurate central difference of a first- and second-order derivatives is used:

$$\frac{\partial u}{\partial x} = \frac{u_{i+1} - u_{i-1}}{2\Delta x} \quad (14)$$

$$\frac{\partial^2 u}{\partial x^2} = \frac{u_{i-1} - 2u_i + u_{i+1}}{\Delta x^2} \quad (15)$$

Using Eqs. (14) and (15), the velocity function in Eq. (6) can be expressed in tri-diagonal matrix form as

$$U(hu)_i = a_i(hu)_{i-1} + b_i(hu)_i + c_i(hu)_{i+1} \quad (16)$$

where

$$a_i = -\frac{(B+1/3)d_i^2}{\Delta x^2} + \frac{d_i}{12\Delta x^2}(-d_{i-1} + d_{i+1}) \quad (17)$$

$$b_i = 1 + \frac{2(B+1/3)d_i^2}{\Delta x^2} \quad (18)$$

$$c_i = -\frac{(B+1/3)d_i^2}{\Delta x^2} - \frac{d_i}{12\Delta x^2}(-d_{i-1} + d_{i+1}) \quad (19)$$

The diagonal elements are time independent and hence the coefficients are evaluated once and the Thomas algorithm is used to solve the tri-diagonal system after the predictor and corrector stages.

TESTS AND RESULTS

The proposed model is first tested for regular wave propagation without considering vegetation in the flow domain. Then the model is applied to reproduce laboratory tests on wave attenuation due to vegetation.

Regular wave propagation over a submerged bar

A very popular laboratory test case introduced by Dingemans (1987) is selected to examine the accuracy of the present model. The same experiments were repeated by Beji and Battjes (1993) and the values recorded are used here for comparison.

The schematic figure of the laboratory set up is shown in Figure 2. All the three tests were simulated but one test case in which spilling breakers are involved is presented here. At the inlet boundary a regular wave with wave height 0.029 m and period 2.525 s is introduced and at the downstream a sponge layer is employed to reduce wave reflection. The numerical flume is discretized using a spatial step of $\Delta x = 0.01$ m. Depth gauges placed along the flume at $x = 2.0, 5.7, 10.5, 13., 15.7$ and 19.0 m record the water surface elevation over time. Figure 3 compares the water surface elevations at different gauges obtained from the experiment and the present model. It should be noted that the phase error recorded at gauge $x = 5.7$ m is attributed to an error in the recording of the experiment (Shiach and Mingham 2009). At all other gauges the model predicts the water surface elevations quite accurately.

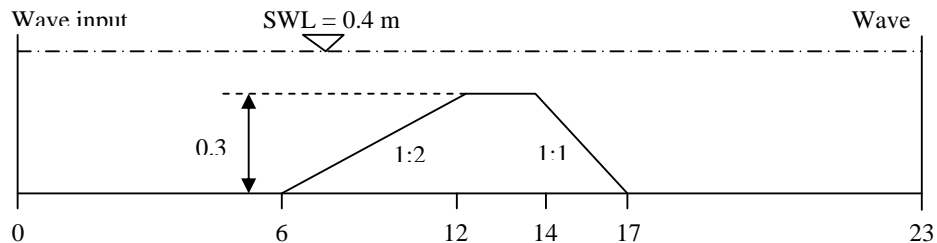


Figure 2. Definition of bed topography for regular wave propagation over a submerged bar

Wave attenuation due to vegetation

Vegetations along a coast have always been regarded as a means of wave attenuation, reducing wave energy as the wave propagates through the vegetations by obstructing the waves with their network of roots and stems. The protection afforded by this shoreline of dense vegetations appears substantial, not only for storm generated waves, winds, typhoons and surges, but also for tsunamis. Thus, more quantitative support has been needed for some time to understand the impact of vegetation on wave attenuation. To investigate how vegetations impact on wave attenuation laboratory tests were conducted at the National Sedimentation Laboratory, Oxford, MS (USA). The experiments were conducted in a wave flume of 20.6 m length, 0.5 m width, and 1.22 m height. The schematic view of the set up is shown in Figure 4. Vegetations are represented by wooden circular cylinder. The stems were fixed to a wire net at the bottom and the length of the vegetation field is $L_V = 3.66$ m. The number density of stems is 350 m^{-2} , length 0.63 m and diameter 9.525 mm. Experiments were carried out with a still water depth 0.7 m. Regular waves of different amplitudes and periods (Table 1) are generated by the wave maker. All the test cases are well within the limit of Boussinesq approximation, i. e. depth to wave length (d/L) ratio is less than 0.5. Five gauges were used to record the water surface elevations at different locations as shown in Figure 4. The numerical model has been set up to replicate the experimental conditions. The computational domain is of length 15.5 m and width 1 m. In the numerical model, the inlet is placed at the location of first gauge because the wave maker sometimes cannot generate waves with exact amplitude and period as

specified through an automatic device controlled by computer. The spatial domain is discretized by $\Delta x = 0.01$ m. At the inlet regular waves are generated and a non-reflecting wave boundary condition is implemented. At the downstream a sponge layer is specified to reduce wave reflection. The wave height at a gauge is calculated from the recorded data and using up crossing method. Six different tests are selected here to reproduce the observed wave heights at different gauges. The comparison of the attenuated wave heights are shown in Figure 5. The coefficient of drag is manipulated by several trials with different values and the best fitting values are reported. It can be concluded from Figure 5 that the present model can reproduce wave attenuation due to vegetation observed at laboratory flume.

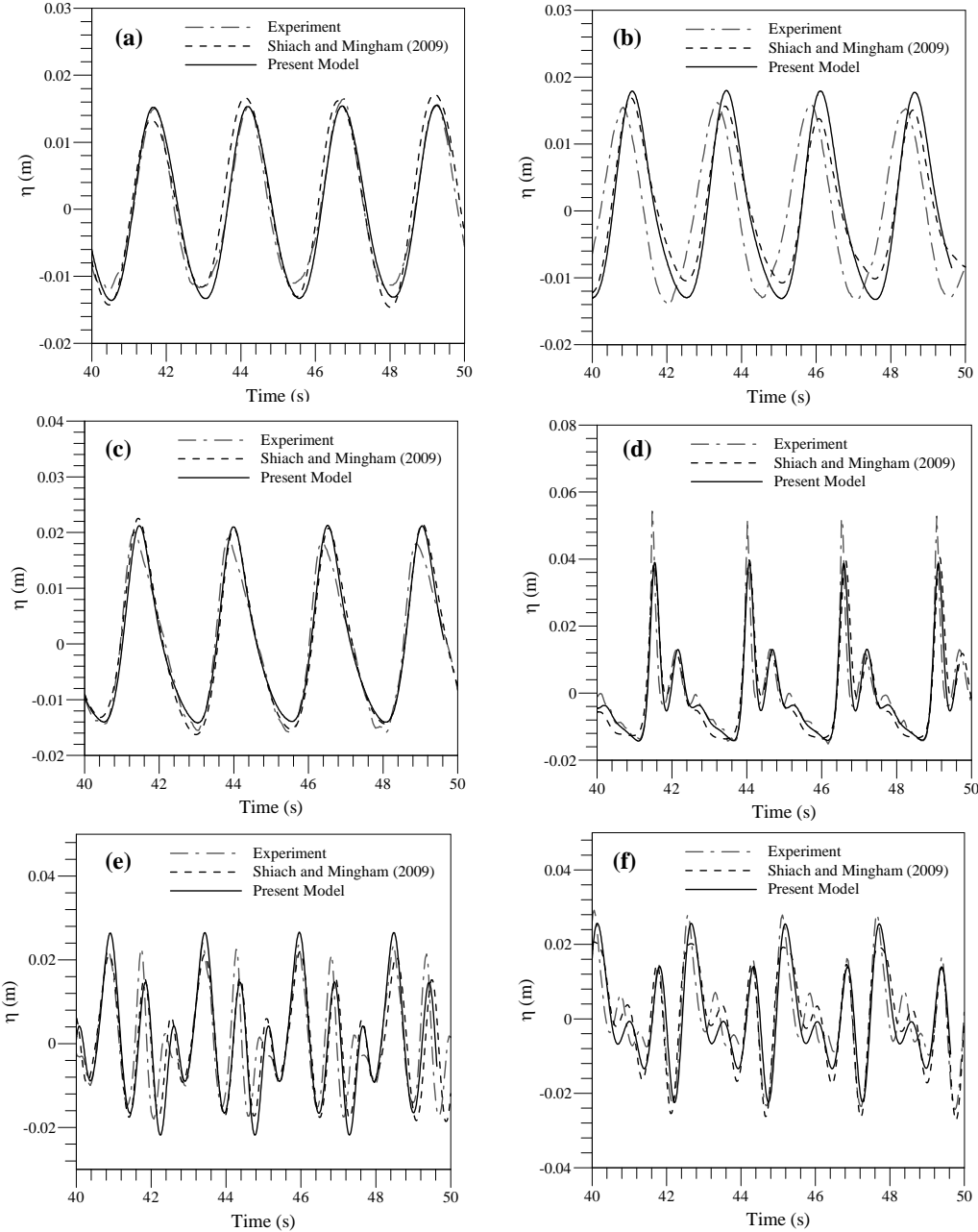


Figure 3. Comparison of water surface elevations at different gauges (a) $x = 2.0$ m, (b) $x = 5.7$ m, (c) $x = 10.5$ m, (d) $x = 13.5$ m, (e) $x = 15.7$ m and (f) $x = 19.0$ m

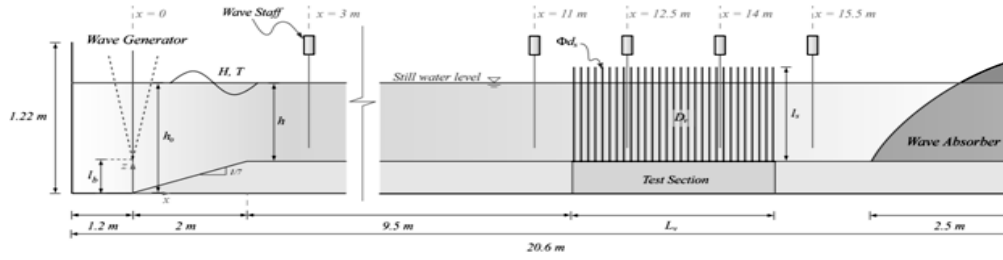
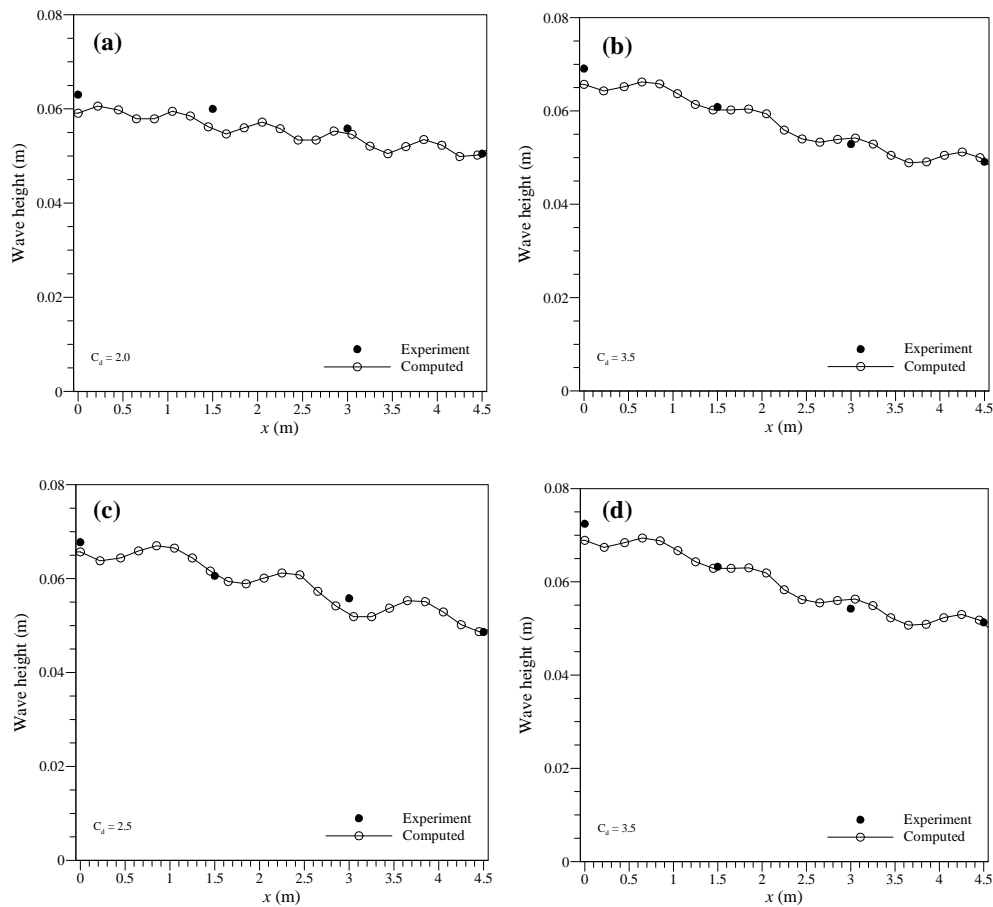


Figure 4. Definition sketch of the laboratory test set up

Configuration	Wave height (m)	Period (s)	d/L
(a)	0.066941	1.2	0.322428
(b)	0.065852	1.4	0.249571
(c)	0.065327	1.6	0.204288
(d)	0.067961	1.4	0.249571
(e)	0.085179	1.6	0.204288
(f)	0.080980	1.2	0.322428

Table 1. Laboratory wave configuration used for the simulation



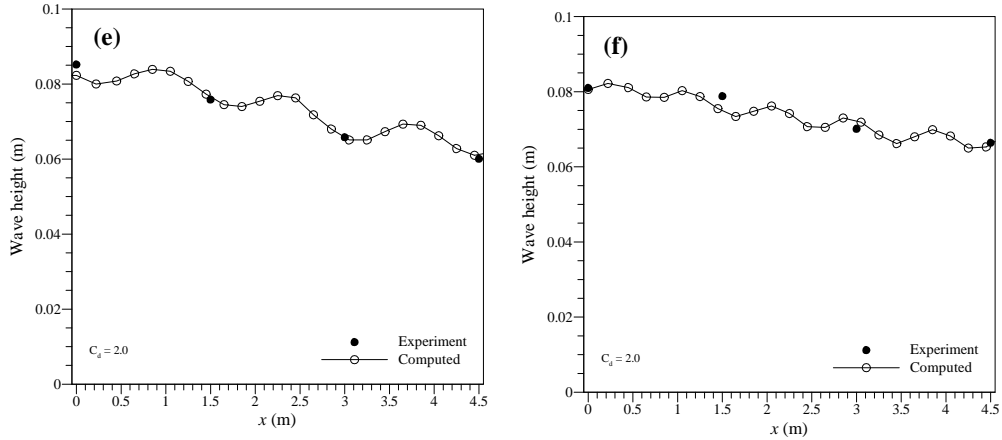


Figure 5. Variation of wave height along the length of the flume for different wave configurations: (a) – (f)

CONCLUSIONS

This paper describes the theoretical background and validation of a one-dimensional shock-capturing Boussinesq wave model to simulate wave run-up and wave attenuation due to vegetation. The model uses the extended Boussinesq equations proposed by Madsen and Sørensen (1992). The system of equations is rearranged in such a way that shock-capturing property can be achieved using a Riemann solver. The proposed model uses a second-order explicit time discretization method and up to a fourth-order accurate space discretization through a piecewise linear reconstruction of the conserved variables. The effect of vegetation is included in the momentum equation as a source term in the form of drag force. The drag force expression considers plant characteristics such as geometry, stem density, spatial coverage etc. to properly represent the physical processes. The numerical model is validated against laboratory test on wave propagation over a submerged bar and good agreement between observed and numerical water surface is obtained. The model is applied to reproduce wave attenuation observed in a wave flume. Six different test cases are simulated and it is found that the model can accurately predict wave attenuation due to vegetation. The model can be further validated against live vegetation and real world scenarios.

ACKNOWLEDGEMENTS

This research was funded by the Department of Homeland Security-sponsored Southeast Region Research Initiative (SERRI) at the Department of Energy's Oak Ridge National Laboratory, USA.

REFERENCES

- Beji, S., and Battjes, J. A. (1993). "Experimental investigations of wave propagation over a bar." *Coast. Eng.*, 19 (1–2), 151–162.
- Dingemans, M. W. (1987). "Verification of numerical wave propagation models with laboratory measurements." Report H228 Part 1. Delft Hydraulics. 400 pp.
- Harten, A., Lax, P., and van Leer, B. (1983). "On upstream differencing and Godunov-type schemes for hyperbolic conservation laws." *SIAM Rev.*, 25, 35–61.
- Madsen, P. A., and Sørensen, O. R. (1992). "A new form of the Boussinesq equations with improved linear dispersion characteristics. Part 2. A slowly-varying bathymetry." *Coast. Eng.*, 18, 183–204.
- Madsen, P. A., Murray, R., and Sørensen, O. R. (1991). "A new form of Boussinesq equations with improved linear dispersion characteristics." *Coast. Eng.*, 15, 371–388.
- Nwogu, O. (1993). "An alternative form of the Boussinesq equations for nearshore wave propagation." *J. Water. Port, Coast. Ocean Eng.*, 119 (6), 618–638.
- Peregrine, D. H. (1967). "Long waves on a beach." *J. Fluid Mech.*, 27 (4), 815–827.
- Shiach, J. B. and Mingham, C. G. (2009). "A temporally second-order accurate Godunov-type scheme for solving the extended Boussinesq equations." *Coastal. Eng.*, 56, 32-45.
- Toro, E. F. (1992). "Riemann problems and the WAF method for solving two-dimensional shallow water equations." *Phil. Trans. Roy. Soc. London, Series A* 338, 843.
- Wei, G., Kirby, J. T., Grilli, S. T., and Subramanya, R. (1995). "A fully nonlinear Boussinesq model for surface waves: part 1. highly nonlinear unsteady waves." *J. Fluid Mech.*, 294, 71–92.
- Yamamoto, S., Kano, S., and Daiguji, H. (1998). "An efficient CFD approach for simulating unsteady hypersonic shock–shock interference flows." *Comput. Fluids*, 27 (5–6), 571–580.
- Zhou, J. G., Causon, D. M., Mingham, C. G., and Ingram, D. M. (2001). "The surface gradient method for the treatment of source terms in the shallow water equations." *J. Comput. Phy.*, 168, 1–25.